ARTICLE

Intraparticle Charge Delocalization through Conjugated Metal-Ligand Interfacial Bonds: Effects of Metal d Electrons[†]

Yi Peng, Eduardo Y. Hirata, Wanzhang Pan, Limei Chen, Jia En Lu, Shaowei Chen*

Department of Chemistry and Biochemistry, University of California, Santa Cruz, California 95064, USA

(Dated: Received on April 19, 2018; Accepted on May 18, 2018)

Intraparticle charge delocalization occurs when metal nanoparticles are functionalized with organic capping ligands through conjugated metal-ligand interfacial bonds. In this study, metal nanoparticles of 5d metals (Ir, Pt, and Au) and 4d metals (Ru, Rh, and Pd) were prepared and capped with ethynylphenylacetylene and the impacts of the number of metal d electrons on the nanoparticle optoelectronic properties were examined. Both FTIR and photoluminescence measurements indicate that intraparticle charge delocalization was enhanced with the increase of the number of d electrons in the same period with palladium being an exception.

Key words: Nanoparticle, d Electron, Acetylene, Interfacial bond, Intraparticle charge delocalization

I. INTRODUCTION

Organically capped transition-metal nanoparticles represent a unique class of functional nanomaterials, where the materials properties can be readily manipulated by the metal core and the organic capping ligands [1−4]. In most prior research, mercapto derivatives have been used extensively for metal nanoparticle surface functionalization, due to the strong affinity of thiol moiety to transition metal surfaces. However, the resulting metal-thiolate (M-S) bonds are known to lack interesting chemistry, thus the impacts of the metal-ligand interfacial bonds on nanoparticle optical and electronic properties have been largely ignored [5, 6]. Recently, new chemistries based on metal-carbon/-nitrogen covalent linkages have been developed for nanoparticle surface functionalization by taking advantage of, for instance, the self-assembly of diazo, olefin, acetylene and azide derivatives on transition-metal surfaces. The formation of metal-carbene (M=C), metal-acetylide/vinylidene (M-C≡/M=C=C), and metal-nitrene (M=N) conjugated linkages leads to efficient intraparticle charge delocalization between the nanoparticle-bound functional moieties and hence the emergence of new optical and electronic properties of the nanoparticles [7−10].

In fact, a series of studies have been carried out with nanoparticles functionalized with acetylene derivatives. For instance, in an earlier study with alkyne-capped ruthenium nanoparticles [11], the specific reactivity of the nanoparticles with imine derivatives suggests the formation of ruthenium-vinylidene (Ru=C=CH-) interfacial bond, which was likely involved in a tautomeric equilibrium with ruthenium-acetylide/-hydride (Ru−C≡/Ru−H). The resulting nanoparticles exhibited unique optical and electronic properties, analogous to those of diacetylene (C≡C−C≡C) derivatives, due to intraparticle charge delocalization between the acetylene moieties. Such nanoparticle-mediate electronic communication may be further manipulated by the valence state of the metal cores [12]. Similar interfacial bonding structures are observed for alkyne-functionalized platinum nanoparticles by using isotope-labeled alkyne ligands [13]. Formation of stable nanoparticles with alkyne surface functionalization has also been reported with other metal nanoparticles, such as Cu, Pd, Ir, Pt, Au, and their alloys [14−20]. In these earlier studies, the interfacial bonding linkages are generally accounted for by the dπ-pπ interactions between the metal cores and the acetylene moiety, where the ligands adopt an end-on configuration. Within such a structural context, apparent impacts are anticipated of the metal d electrons on the interfacial bonding interactions, a topic that has not been systematically examined thus far. This is the primary motivation of the present study.

Herein, a range of transition-metal nanoparticles, including 4d metals of Ru ($5s^14d^7$), Rh ($5s^14d^8$) and Pd ($5s^04d^{10}$), and 5d metals of Ir ($6s^24f^{14}5d^7$), Pt ($6s^14f^{14}5d^9$) and Au ($6s^14f^{14}5d^{10}$), were prepared and capped with ethynylphenylacetylene (EPA). The mor-

[†]Part of the special issue for celebration of "the 60th Anniversary of University of Science and Technology of China and the 30th Anniversary of Chinese Journal of Chemical Physics".

*Author to whom correspondence should be addressed. E-mail: shaowei@ucsc.edu

 ©2018 Chinese Physical Society

phology and size of these metal nanoparticles were characterized by transmission electron microscopic measurements, and the optical and electronic properties of the nanoparticles were measured by spectroscopic techniques, where the signatory features for intraparticle charge delocalization were quantified by FTIR and photoluminescence measurements, and compared within the context of the metal d electrons. The results indicate that intraparticle delocalization increases with increasing number of d electrons for metals in the same period, with palladium being an exception due to its unusual electron affinity as compared to other 4d metals.

II. EXPERIMENTS

A. Chemicals

Ruthenium(III) chloride ($RuCl_3$, 35%−40% Ru, Acros), rhodium(III) chloride ($RhCl_3$, 48.6%−49.2% Rh, Acros), palladium(II) chloride ($PdCl_2$, 59%−60% Pd, Acros), iridium(III) chloride ($IrCl_3$, 53%−56% Ir, Acros), platinum(IV) chloride ($PtCl_4$, 57.0%−58.5% Pt, Acros), hydrogen tetrachloroauric acid ($HAuCl_4{\cdot}4H_2O$, 99.9%, Sigma-Aldrich), sodium borohydride ($NaBH_4$, 99%, Acros), polyvinylpyrrolidone (PVP, MW 40,000, USB), and 4-ethynylphenylacetylene (EPA, 97%, Acros) were used as received. Solvents were purchased at the highest purity available from typical commercial sources and also used as received. Water was deionized with a Barnstead Nanopure Water System (18.3 MΩ·cm).

B. Synthesis of Ru, Rh, Ir, and Pt nanoparticles

Ru, Rh, Ir, and Pt nanoparticles were synthesized by adopting a literature protocol with some modifications [21]. Briefly, 0.3 mmol of the respective metal chloride ($RuCl_3$, $RhCl_3$, $IrCl_3$, and $PtCl_4$) were dissolved in 5 mL of nanopure water and added into 100 mL of ethylene glycol under vigorous stirring, into which was then added 5 mL of a 0.5 mol/L NaOH solution. Metal nanoparticles were produced by heating the solution at 160 °C for 3 h, as signified by the apparent color change of the solution to dark brown. After the solution was cooled down to room temperature, 50 mL of toluene and 0.9 mmol of EPA (corresponding to an EPA to metal mole ratio of 3:1) were added into the solution under magnetic stirring. The mixing was run at 60 °C for 12 h, and the nanoparticles were found to be transferred into the toluene phase. The toluene phase was collected, dried by rotary evaporation, and rinsed extensively with methanol to obtain purified metal nanoparticles, which were denoted as RuEPA, RhEPA, IrEPA, and PtEPA, respectively.

C. Synthesis of Pd and Au nanoparticles

Au and Pd nanoparticles were prepared by following another literature procedure with some modifications [14]. Briefly, 200 mg of PVP was dissolved in 45 mL of nanopure water and mixed with 45 mL of 2 mmol/L $HAuCl_4$ or H_2PdCl_4. The solution was kept in an ice bath for 30 min, into which was then added 5 mL of a $NaBH_4$ solution (7 mg/mL) under magnetic stirring for 15 min. After the product was warmed up to room temperature, 45 mL of toluene and 0.27 mmol of EPA (corresponding to an EPA to metal mole ratio of 3:1) were added into the solution under magnetic stirring. The mixing was run at 60 °C for 12 h, and the nanoparticles were found to be transferred into the toluene phase. The toluene phase was collected, dried by rotary evaporation, and rinsed extensively with methanol to afford purified PdEPA and AuEPA nanoparticles.

D. Characterizations

The morphology and size of the obtained nanoparticles were characterized by transmission electron microscopic (TEM) measurements (Philips CM300 at 300 kV). FTIR measurements were carried out with a Perkin Elmer FTIR spectrometer (Spectrum One, spectral resolution 1 cm^{-1}), where the samples were prepared by drop-casting the nanoparticle solution onto a ZnSe disk. UV-Vis spectra were collected with a Perkin Elmer Lambda 35 UV-Vis spectrometer, and the same solutions were used for photoluminescence measurements which were performed with a PTI fluorospectrometer.

III. RESULTS AND DISCUSSION

The structure of the EPA-capped nanoparticles was first examined by TEM measurements. As shown in FIG. 1(A1−F1), all nanoparticles were well-dispersed without apparent aggregation, suggesting good protection of the metal nanoparticles by the EPA ligands. In high-resolution TEM studies (FIG. 1(A2−F2)), the M-EPA nanoparticles all exhibited well-defined lattice fringes of the metal cores, with the interplanar spacings in good agreement with their bulk fcc crystalline structures: 0.234 nm for Ru(100) (JCPDS card No. 88-2333, FIG. 1(A2)) [22], 0.220 nm for Rh(111) (JCPDS card No. 5-685, FIG. 1(B2)) [23], 0.226 nm for Pd (111) (JCPDS card No. 46-1043, FIG. 1(C2)) [24], 0.225 nm for Ir(111) (JCPDS card No. 46-1044, FIG. 1(D2) [24], 0.230 nm for Pt(111) (JCPDS card No. 4-802, FIG. 1(E2)) [24], and 0.235 nm for Au(111) (JCPDS card No. 4-784, FIG. 1(F2)) [24]. Furthermore, statistical analysis based on more than 100 nanoparticles was carried out to quantify the metal core sizes. From the core size histograms in FIG. 1(A3−F3), one can see that the nanoparticles all fell within a rather narrow core size range, and the average diameter was esti-

DOI:10.1063/1674-0068/31/cjcp1804073 ©2018 Chinese Physical Society

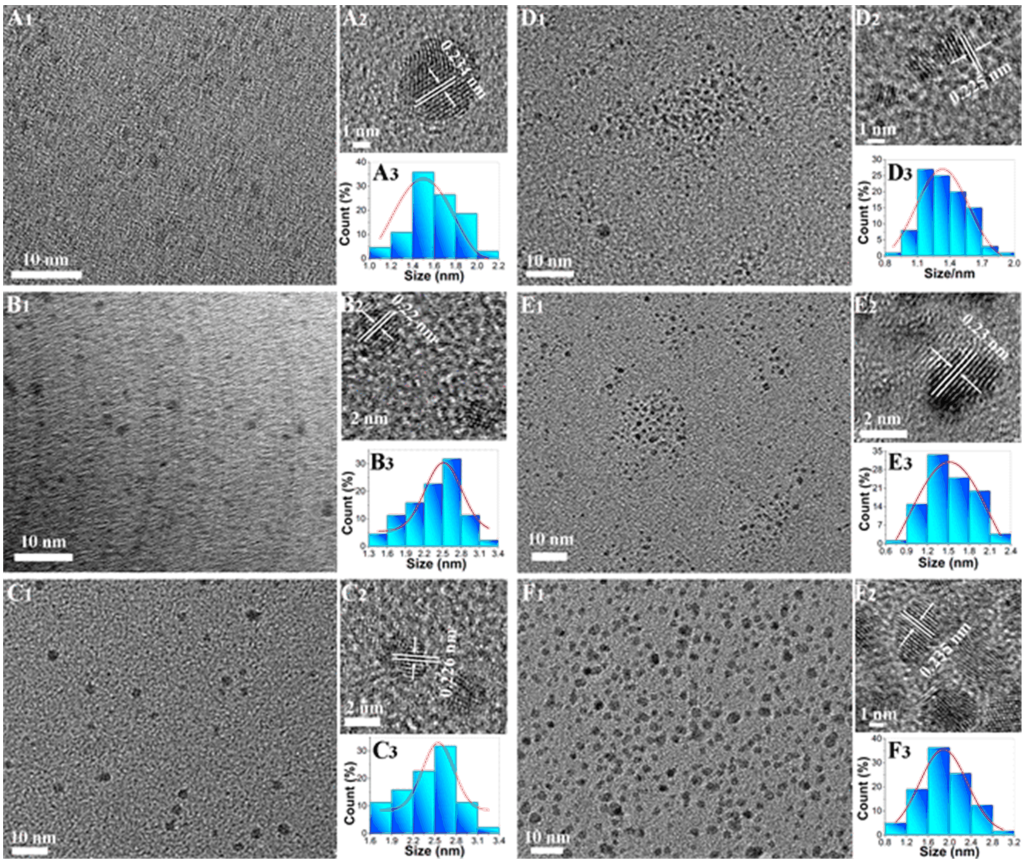

FIG. 1 Representative TEM images of the EPA-capped nanoparticles: (A1, A2) Ru, (B1, B2) Rh, (C1, C2) Pd, (D1, D2) Ir, (E1, E2) Pt, and (F1, F2) Au. The corresponding core size histograms are shown in panels (A3−F3).

mated to be 1.55±0.37 nm for RuEPA, 2.30±0.60 nm for RhEPA, 2.50±0.56 nm for PdEPA, 1.37±0.37 nm for IrEPA, 1.55±0.46 nm for PtEPA, and 2.20±0.64 nm for AuEPA (Table I). That is, for metals in the same period, the average core size of the nanoparticles increased with an increase of the number of the metal d electrons; whereas for metals in the same groups, the nanoparticles of 5d metals are generally somewhat smaller than those of the 4d counterparts. Such observations may be accounted for, at least in part, by the metal-metal bond dissociation energy that decreases from the left (bottom) to the right (top) of the periodical table [25], as smaller nanoparticles are more likely to be formed with stronger metal-metal bonds due to enhanced nucleation of metal atoms [26].

The elemental compositions and valance states of carbons and metals in the nanoparticles were then examined by XPS measurements. As depicted in FIG. 2 (A) and (C), the series of nanoparticle samples all exhibit two peaks for the C 1s electrons, the main one centered at about 284.40 eV, which can be ascribed to the combined contributions of sp- (C≡C) and sp^2-hybridized (phenyl ring) carbons, and a minor one at ca. 285.62 eV due to sp^3 carbons (C−C) of the EPA ligands (another weak one can be seen at ca. 288.0 eV, which most likely arose from C=O of impurities adsorbed on the metal nanoparticle surface). FIG. 1(B) displays the scans of the metal 3d electrons of RuEPA, RhEPA and PdEPA nanoparticles, and the $3d_{5/2}/3d_{3/2}$ binding energies can be identified at 280.77/284.87, 307.97/312.72, and 336.01/341.26 eV, respectively. Similarly, FIG. 2(D) shows the spectra of the metal 4f electrons of IrEPA, PtEPA, and AuEPA nanoparticles, where the $4f_{7/2}/4f_{5/2}$ peaks can be found at 61.40/64.37, 71.83/75.10, and 84.05/87.71 eV, respectively. Note these values are somewhat higher than those of the respective bulk metal $3d_{5/2}/3d_{3/2}$ or $4f_{7/2}/4f_{5/2}$ energies, which are 280.0/284.1, 307.0/311.75, 334.9/340.15, 60.6/63.55, 70.9/74.25, and 83.8/87.45 eV for Ru, Rh, Pd, Ir, Pt and Au [27], respectively. This may be accounted for by the back-donation of metal d electrons to the π^* orbital of the acetylene moieties in the bonding interactions between the metal cores and acetylene ligands, resulting in electron-deficient metal cores in the nanoparticles [28, 29]. The surface structures of the EPA functionalized metal nanoparticles were further studied by FTIR measurements. As observed previously [11, 13, 30, 31], the ≡C−H vibration that is clearly defined at 3287 cm^{-1} for monomeric EPA vanished for all nanoparticles, suggesting effective cleavage of

DOI:10.1063/1674-0068/31/cjcp1804073 ©2018 Chinese Physical Society

TABLE I Summary of FTIR and photoluminescence properties of EPA-capped metal nanoparticles

	Metal electronic configuration	Electron affinity/ (kJ/mol) [44]	Core diameter/ nm	Aromatic ring $\nu_{=C\text{-}H}/cm^{-1}$	λ_{ex}/nm	λ_{em}/nm
EPA				3026		
RuEPA	$[Kr]5s^14d^7$	101.1	1.55±0.37	3021	381	458
RhEPA	$[Kr]5s^14d^8$	109.7	2.30±0.60	3019	390	479
PdEPA	$[Kr]5s^04d^{10}$	54.2	2.50±0.56	3022	370	452
IrEPA	$[Xe]6s^24f^{14}5d^7$	151.0	1.37±0.37	3023	334	388
PtEPA	$[Xe]6s^14f^{14}5d^9$	205.3	1.55±0.46	3021	338	399
AuEPA	$[Xe]6s^14f^{14}5d^{10}$	222.7	2.20±0.64	3020	343	403

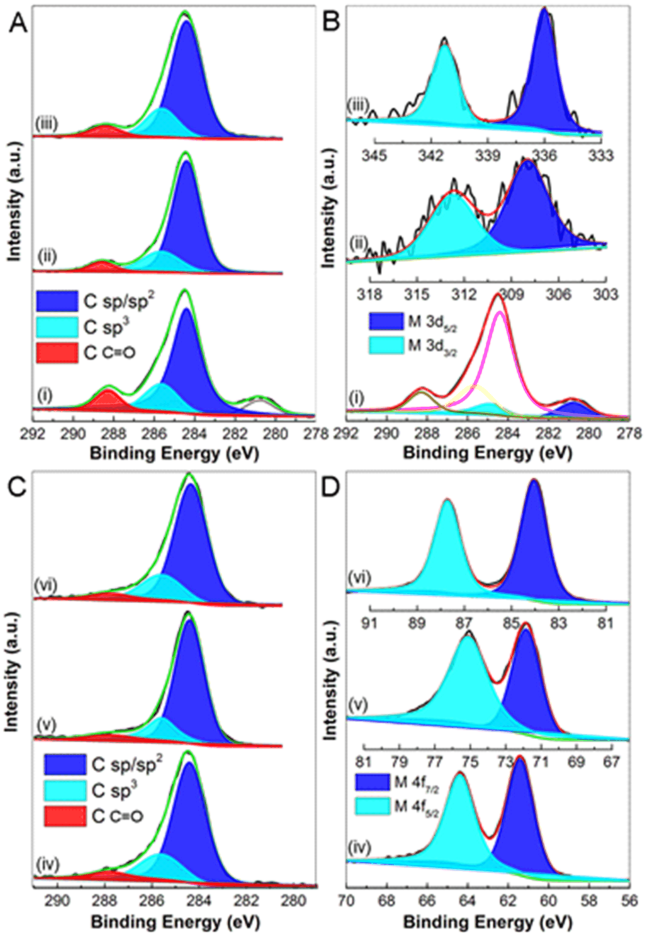

FIG. 2 High-resolution XPS scans of (A) C 1s and (B) metal 3d electrons of (i) RuEPA, (ii) RhEPA and (iii) PdEPA nanoparticles, and (C) C 1s and (D) metal 4f electrons of (iv) IrEPA, (v) PtEPA, and (vi) AuEPA.

the ≡C−H bonds during ligand self-assembly onto the nanoparticle surface, likely forming metal-vinylidene/-acetylide interfacial bonds. In fact, the vibrational bands of the methylene groups of the EPA ligands can be readily identified for all nanoparticle samples in the range of 2800 cm^{-1} to 3000 cm^{-1}; yet, the phenyl ring =C−H vibration displays a clear red-shift as compared

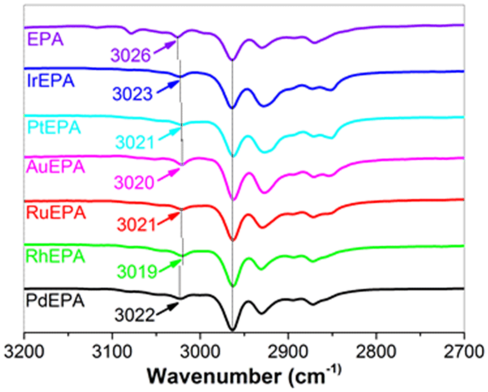

FIG. 3 FTIR spectra of M-EPA nanoparticles in the range of 2700 cm^{-1} to 3200 cm^{-1}.

to that (3026 cm^{-1}) of the EPA monomers (FIG. 3): 3023 cm^{-1} for IrEPA, 3021 cm^{-1} for PtEPA, 3020 cm^{-1} for AuEPA, 3021 cm^{-1} for RuEPA, 3019 cm^{-1} for RhEPA, and 3022 cm^{-1} for PdEPA (Table I). This indicates that the bonding order of phenyl =C−H decreases upon the adsorption of the EPA ligands onto the metal nanoparticle surface, most likely due to the formation of conjugated metal-ligand interfacial bonds that leads to effective intraparticle charge delocalization between the particle-bound functional moieties; and the red-shift was slightly enhanced with increasing number of d electrons for both 4d and 5d metals (with Pd being the exception). As mentioned earlier, the metal-ligand interfacial bonds have been accounted for by dπ-pπ interactions, where the donation of carbon π electrons to the metal empty d orbitals produces the σ bond and back-donation of metal d electrons to the carbon π* orbital forms the π component [11, 32−35]. Therefore, one can see that an increase of the number of metal d electrons would strengthen the metal-ligand interfacial linkages and concurrently diminish the carbon bonding order, in good agreement with the FTIR experimental results observed above. Similar results have also been observed with vinylanthracene-functionalized ruthenium nanoparticles [36], and ethynylferrocene-functionalized Pt nanoparticle and nanoclusters [37].

Interestingly, corresponding variations can be seen in

DOI:10.1063/1674-0068/31/cjcp1804073 ©2018 Chinese Physical Society

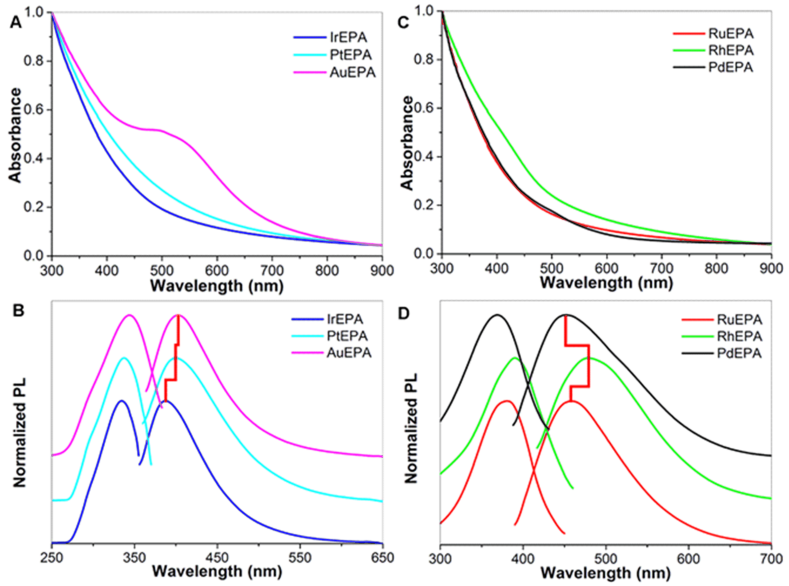

FIG. 4 (A, C) UV-Vis and (B, D) PL spectra of EPA-capped metal nanoparticles in $CHCl_3$. (A, B) 5d metals of Ir, Pt and Au, and (C, D) 4d metals of Ru, Rh and Pd. The PL intensity has been normalized to the optical density at the respective excitation wavelength.

the optical properties of the nanoparticles. FIG. 4(A) depicts the UV-Vis absorption spectra of the nanoparticle samples of 5d metals. Both IrEPA and PtEPA nanoparticles exhibited an exponential decay profile that is consistent with the Mie characteristics of metal nanoparticle, while AuEPA nanoparticles displayed an absorption peak centered at 510 nm due to surface plasmon resonance [38, 39]. These nanoparticles also exhibit apparent photoluminescence emission (FIG. 4(B)), which has been accounted for by the formation of conjugated metal-ligand interfacial bonds that leads to effective intraparticle charge delocalization between the particle-bound acetylene moieties, such that they behave analogously to diacetylene (C≡C−C≡C) derivatives [37, 40−43]. Yet a close analysis shows that the excitation (λ_{ex}) and emission (λ_{em}) peak positions actually vary slightly among the samples: 334 nm and 388 nm for IrEPA, 338 nm and 399 nm for PtEPA, and 343 nm and 403 nm for AuEPA (highlighted by red lines in FIG. 3(B)). That is, the peak positions red-shift with the increase of the number of metal 5d electrons. Similar behaviors can be seen with 4d metal nanoparticles, as depicted in FIG. 4 (C) and (D). One can see that RuEPA, RhEPA and PdEPA nanoparticles also exhibited an exponential decay profile, along with a red-shift of the excitation and emission maxima (with PdEPA being the exception): 381 nm and 458 nm for RuEPA, 390 nm and 479 nm for RhEPA, and 370 nm and 452 nm for PdEPA. These results (Table I), again, suggest increasing intraparticle conjugation for 5d and 4d metals to the right of the periodical table.

It should be noted that results in the above FTIR and photoluminescence measurements are also consistent with electron affinity (Table I) of the metals, which is 101.1 kJ/mol for Ru, 109.7 kJ/mol for Rh, 54.2 kJ/mol for Pd, 151.0 kJ/mol for Ir, 205.3 kJ/mol for Pt and 222.7 kJ/mol for Au, in which Pd is an exception [44]. That is, it is most likely that the low electron affinity of Pd diminishes the metal-ligand interfacial bond, leading to weakened intraparticle charge delocalization, as manifested in a blue-shift of the aromatic =C−H vibrational stretch and the photoluminescence emission.

IV. CONCLUSION

Stable nanoparticles of select 4d and 5d metals were prepared by the self-assembly of EPA ligands onto the nanoparticle surface, forming metal-vinylidene interfacial bonds. Spectroscopic measurements show that the intraparticle charge delocalization increased with an increase of the number of metal d electrons in the same period, due to enhanced pπ-dπ interactions between the metal cores and carbon π electrons. Pd is an exception within this context, which was accounted for by the unusually low electron affinity that leads to weakened interfacial bonds and hence intraparticle charge delocalization. Results from these studies may offer new fundamental insights into organic functionalization of metal nanoparticles and the manipulation of the optical and electronic properties.

V. ACKNOWLEDGMENTS

This work was supported, in part, by the National Science Foundation (DMR-1409396 and CHE-1710408). TEM and XPS work was carried out at the National

DOI:10.1063/1674-0068/31/cjcp1804073 ©2018 Chinese Physical Society

Center for Electron Microscopy and Molecular Foundry of Lawrence Berkeley National Laboratory, which is supported by the US Department of Energy.

[1] R. W. Murray, Chem. Rev. **108**, 2688 (2008).
[2] R. Mout, D. F. Moyano, S. Rana, and V. M. Rotello, Chem. Soc. Rev. **41**. 2539 (2012).
[3] Y. Wang, X. K. Wan, L. Ren, H. Su, G. Li, S. Malola, S. Lin, Z. Tang, H. Hakkinen, B. K. Teo, Q. M. Wang, and N. Zheng, J. Am. Chem. Soc. **138**, 3278 (2016).
[4] D. J. Gavia and Y. S. Shon, Chemcatchem **7**, 892 (2015).
[5] H. Hakkinen, Nat. Chem. **4**, 443 (2012).
[6] K. Saha, S. S. Agasti, C. Kim, X. Li, and V. M. Rotello, Chem. Rev. **112**, 2739 (2012).
[7] P. G. Hu, L. M. Chen, X. W. Kang, and S. W. Chen, Acc. Chem. Res. **49**, 2251 (2016).
[8] L. M. Chen, P. G. Hu, C. P. Deming, W. Li, L. G. Li, and S. W. Chen, J. Phys. Chem. C **119**, 15449 (2015).
[9] L. M. Chen, Y. Song, P. G. Hu, C. P. Deming, Y. Guo, and S. W. Chen, Phys. Chem. Chem. Phys. **16**, 18736 (2014).
[10] C. P. Deming, X. W. Kang, K. Liu, and S. W. Chen, Sensors Actuat. B-Chem. **194**, 319 (2014).
[11] X. W. Kang, N. B. Zuckerman, J. P. Konopelski, and S. W. Chen, J. Am. Chem. Soc. **134**, 1412 (2012).
[12] X. W. Kang, N. B. Zuckerman, J. P. Konopelski, and S. W. Chen, Angew. Chem. Int. Edit. **49**, 9496 (2010).
[13] P. G. Hu, L. M. Chen, C. P. Deming, L. W. Bonny, H. W. Lee, and S. W. Chen, Chem. Commun. **52**, 11631 (2016).
[14] P. Maity, H. Tsunoyama, M. Yamauchi, S. Xie, and T. Tsukuda, J. Am. Chem. Soc. **133**, 20123 (2011).
[15] H. Yamamoto, P. Maity, R. Takahata, S. Yamazoe, K. Koyasu, W. Kurashige, Y. Negishi, and T. Tsukuda, J. Phys. Chem. C **121**, 10936 (2017).
[16] Y. Wang, H. Su, C. Xu, G. Li, L. Gell, S. Lin, Z. Tang, H. Hakkinen, and N. Zheng, J. Am. Chem. Soc. **137**, 4324 (2015).
[17] P. G. Hu, L. M. Chen, C. P. Deming, X. W. Kang, and S. W. Chen, Angew. Chem. Int. Edit. **55**, 1455 (2016).
[18] C. P. Deming, A. Zhao, Y. Song, K. Liu, M. M. Khan, V. M. Yates, and S. W. Chen, Chemelectrochem **2**, 1719 (2015).
[19] K. Liu, Y. Song, and S. W. Chen, J. Power Sources **268**, 469 (2014).
[20] P. G. Hu, Y. Song, L. M. Chen, and S. W. Chen, Nanoscale **7**, 9627 (2015).
[21] Y. Wang, J. W. Ren, K. Deng, L. L. Gui, and Y. Q. Tang, Chem. Mater. **12**, 1622 (2000).
[22] H. H. Ye, Q. X. Wang, M. Catalano, N. Lu, J. Vermeylen, M. J. Kim, Y. Z. Liu, Y. G. Sun, and X. H. Xia, Nano Lett. **16**, 2812 (2016).
[23] A. J. Biacchi and R. E. Schaak, ACS Nano **5**, 8089 (2011).
[24] X. Wang, J. Zhuang, Q. Peng, and Y. D. Li, Nature **437**, 121 (2005).
[25] D. R. Lide, *CRC Handbook of Chemistry and Physics: a Ready-Reference Book of Chemical and Physical Data*, 85th Edn., Boca Raton, Fla CRC Press, (2004).
[26] S. W. Chen, A. C. Templeton, and R. W. Murray, Langmuir **16**, 3543 (2000).
[27] C. D. Wanger, W. M. Riggs, L. E. Davis, M. J. F, and G. E. Muilenberg, *Handbook of X-ray Photoelectron Spectroscopy*. Eden Prairie, Minnesota, USA: Perkin-Elmer Corp., Physical Electronics Division, (1979).
[28] F. Zhang, L. Huang, J. Zou, J. Yan, J. Zhu, X. Kang, and S. Chen, J. Nanopart. Res. 19 (2017).
[29] A. A. Khassin, T. M. Yurieva, V. V. Kaichev, V. I. Bukhtiyarov, A. A. Budneva, E. A. Paukshtis, and V. N. Parmon, J. Molec. Catal. A: Chem. **175**, 189 (2001).
[30] K. Liu, X. W. Kang, Z. Y. Zhou, Y. Song, L. J. Lee, D. Tian, and S. W. Chen, J. Electroanal. Chem. **688**, 143 (2013).
[31] C. Bianchini, M. Peruzzini, A. Vacca, and F. Zanobini, Organometallics **10**, 3697 (1991).
[32] Y. Wakatsuki, N. Koga, H. Yamazaki, and K. Morokuma, J. Am. Chem. Soc. **116**, 8105 (1994).
[33] C. Slugovc, V. N. Sapunov, P. Wiede, K. Mereiter, R. Schmid, and K. Kirchner, J. Chem. Soc. Dalton Trans. 4209 (1997).
[34] Y. Wakatsuki, J. Organomet. Chem. **689**, 4092 (2004).
[35] H. Braunschweig, Q. Ye, A. Vargas, R. D. Dewhurst, K. Radacki, and A. Damme, Nat. Chem. **4**, 563 (2012).
[36] W. Chen, S. Pradhan, and S. W. Chen, Nanoscale **3**, 2294 (2011).
[37] P. Hu, L. Chen, C. P. Deming, X. Kang, and S. Chen, Angew. Chem. Int. Edit. 55, 1455 (2016).
[38] G. Mie, Ann Phys-Berlin **25**, 377 (1908).
[39] S. Eustis and M. A. El-Sayed, Chem. Soc. Rev. **35**, 209 (2006).
[40] P. G. Hu, L. M. Chen, C. P. Deming, J. E. Lu, L. W. Bonny, and S. W. Chen, Nanoscale **8**, 12013 (2016).
[41] W. Chen, N. B. Zuckerman, X. W. Kang, D. Ghosh, J. P. Konopelski, and S. W. Chen, J. Phys. Chem. C **114**, 18146 (2010).
[42] H. K. Black, D. H. S. Horn, and B. C. L. Weedon, J. Chem. Soc. **1704** (1954).
[43] R. Warta and H. Sixl, J Chem Phys **88**, 95 (1988).
[44] N. L. Abbott and G. M. Whitesides, Langmuir **10**, 1493 (1994).

Shaowei Chen received his B.S. degree in Chemistry from the University of Science and Technology of China (USTC, Class 8603) in 1991, and his M.S. and Ph.D. degrees from Cornell University in 1993 and 1996, respectively. Following a postdoctoral appointment in the University of North Carolina at Chapel Hill, he started his independent career in Southern Illinois University-Carbondale in 1998. In 2004, he moved to the University of California-Santa Cruz (UCSC). He is currently a Professor of Chemistry and the Faculty Director of the UCSC COSMOS program. His research interests are primarily focused on the design and engineering of high-performance catalysts for electrochemical energy conversion and storage, impacts of metal-ligand interfacial bonding interactions on nanoparticle charge-transfer dynamics, Janus nanoparticles by interfacial engineering, and antimicrobial activity of functional nanomaterials.

DOI:10.1063/1674-0068/31/cjcp1804073 ©2018 Chinese Physical Society